Journal of *Marine Science and Engineering*

MDPI

Article

Long-Term Variability and Trends in Extreme Wave Climate Along the Bay of Biscay

Manuel Viñes [1,2,*], César Mösso [1,2], Felícitas Calderón-Vega [3,*], Benjamí Calvillo [1,2], Marc Mestres [1,2] and Agustín Sánchez-Arcilla [1,2]

[1] Laboratori d'Enginyeria Marítima, Department of Civil and Environmental Engineering, Civil Engineering School (Campus Nord), Universitat Politècnica de Catalunya BarcelonaTech, c/Jordi Girona 1-3, 08034 Barcelona, Spain; cesar.mosso@upc.edu (C.M.); benjami.calvillo@upc.edu (B.C.); marc.mestres@upc.edu (M.M.); agustin.arcilla@upc.edu (A.S.-A.)

[2] Centre Internacional d'Investigació dels Recursos Costaners (CIIRC), c/Jordi Girona 1-3, Mòdul D1, 08034 Barcelona, Spain

[3] Department of Civil and Environmental Engineering, Universidad de Guanajuato, Juárez 77, Zona Centro, Guanajuato 36000, Mexico

* Correspondence: manuel.vines@upc.edu (M.V.); f.calderon@ugto.mx (F.C.-V.)

Abstract

Detecting long-term changes in extreme wave climate is essential for coastal engineering and hazard assessment, yet robust trend identification remains challenging due to strong natural variability and limited observational records. This study evaluates the robustness of trend detection in wave conditions along the Bay of Biscay using in situ measurements for a direct comparison with atmospheric climate indices such as North Atlantic Oscillation (NAO), East Atlantic pattern (EA), and El Niño-Southern Oscillation index (ENSO). A 32-year-long deep-water buoy record of wave parameters (1990–2022) is first analyzed and systematically compared with a nearby and shorter record (2007–2018) to quantify the influence of record length on extreme value estimates and trend inference. Extreme events are identified using a peak-over-threshold approach, and trends in significant wave height (H_S), peak period (T_P), wave steepness (S), and storm-related metrics are assessed through non-parametric methods. No statistically significant long-term trend is detected in the monthly averaged H_S. In contrast, significant increases are found in storm frequency and storm wave power, together with a decreasing trend in T_P and increasing wave steepness, indicating changes in storminess rather than in wave height alone. The shorter record exhibits substantially wider confidence intervals in return levels and inconsistent trend signals, highlighting the structural sensitivity of statistics to temporal coverage. Additionally, correlation analysis with large-scale atmospheric indices reveals that wave-parameters variability is more closely associated with the EA pattern than with the NAO or the ENSO, although the overall explained variance remains limited.

Keywords: extreme wave climate; storm activity; cross-correlation; Bay of Biscay

Check for updates

Academic Editor: Mike Meylan

Received: 5 March 2026
Revised: 26 March 2026
Accepted: 29 March 2026
Published: 31 March 2026

Copyright: © 2026 by the authors. Licensee MDPI, Basel, Switzerland. This article is an open access article distributed under the terms and conditions of the Creative Commons Attribution (CC BY) license.

1. Introduction

Extreme wave conditions play a fundamental role in coastal morphodynamics, structural loading, and coastal hazard assessment [1,2]. Storm-induced changes can translate into measurable morphodynamic responses (e.g., sandbar migration), even in the absence of clear trends in mean significant wave height (H_S), highlighting the need to examine multiple wave parameters when assessing coastal impacts [3–5]. Reliable estimates of

extreme wave heights and storm characteristics are therefore essential for the design and safety assessment of coastal and offshore infrastructure, particularly along exposed mid-latitude coastlines influenced by meso-tidal and intense storms [6]. In recent decades, increased attention has been paid to the possibility of long-term changes in wave climate, motivated by observed and projected modifications in large-scale atmospheric circulation and ocean-atmosphere coupling [7,8].

However, both the magnitude and direction of reported trends often differ across studies, highlighting the sensitivity of wave climate assessment to methodological choices and data availability, particularly in the North Atlantic, where climate variability is strongly modulated by large-scale atmospheric indices [9,10]. In the Bay of Biscay, storm directionality and wave energy data are often spatially heterogeneous and sensitive to the period analyzed [11].

Previous studies have reported inconsistent trends in wave climate parameters, largely depending on data source, analyzed period, and spatial variability (e.g., [12]). This uncertainty is particularly relevant in regions such as the Bay of Biscay, where strong natural variability and large-scale atmospheric oscillations hinder the detection of robust long-term changes (e.g., [11,13–15]). More broadly, this sensitivity reflects a key challenge in wave climate studies: the coexistence of strong natural variability, multi-decadal atmospheric oscillations, and relatively short observational records, as previously pointed out by other studies relating large-scale atmospheric forcing to local wave conditions [16].

Large-scale atmospheric modes such as the North Atlantic Oscillation (NAO) and the East Atlantic pattern (EA) are known to exert a strong control on wind fields and storm tracks over the North Atlantic [17]. Their influence on wave generation and propagation has been documented in several studies, showing statistically significant relationships between atmospheric circulation indices and wave parameters, particularly during winter months [18,19]. Beyond these regional modes, climate variability associated with the El Niño-Southern Oscillation (ENSO) has also been suggested to modulate North Atlantic atmospheric circulation through large-scale teleconnection patterns, although its impact on wave conditions in the northeast Atlantic is generally weaker, indirect, and often characterized by time-lagged responses [20,21]. Assessing the robustness of detected trends and correlations, therefore, requires not only appropriate statistical methods, but also an explicit evaluation of the influence of record length and temporal coverage, which remains insufficiently addressed in many existing studies and motivates the present work [22–24].

Despite extensive research on wave climate variability in the North Atlantic, the structural sensitivity of trend detection to record length and parameter selection has rarely been assessed under identical methodological frameworks. Most regional studies implicitly assume that H_S provides an adequate proxy for changes in the extreme wave climate. However, as H_S represents an integrated bulk parameter derived from the zeroth spectral moment, it does not resolve how wave energy is distributed across frequencies [25,26]. Consequently, structurally different sea states may exhibit comparable H_S values despite substantial differences in spectral shape. Climate-driven modifications in storm intensity, duration, or fetch can induce shifts in peak period and wave steepness without necessarily producing proportional changes in total wave energy. Such spectral adjustments may therefore reveal emerging trends in storminess and wave dynamics earlier, or more robustly, than bulk statistics alone.

The main contribution of this study is the explicit assessment of how record length affects the stability of trend detection and extreme value estimation across multiple wave parameters under a consistent statistical framework. By jointly analyzing H_S, wave peak period (T_P), wave steepness (S), and storm-related metrics, this approach allows us to distinguish robust physical signals from artifacts associated with limited temporal coverage.

Accordingly, the objectives of this study are to (i) characterize variability and trends in offshore wave and storm-related parameters along the Bay of Biscay; (ii) quantify the impact of record length on detected trends, return levels and their uncertainties; and (iii) assess the modulation of wave variability by large-scale atmospheric circulation indices (NAO, EA and ENSO).

2. Study Area

2.1. Geographical Framework

The study area is located in the southeastern Bay of Biscay, focusing on the Basque Country coastline and the surroundings of the Bilbao harbor and the Nervión Estuary (approx. 43°20′ N, 3°01′ W), as shown in Figure 1. This North Atlantic region features a narrow continental shelf, ranging from 7 to 20 km in width, and a rugged coastline characterized by rocky cliffs interspersed with pocket beaches [9,27].

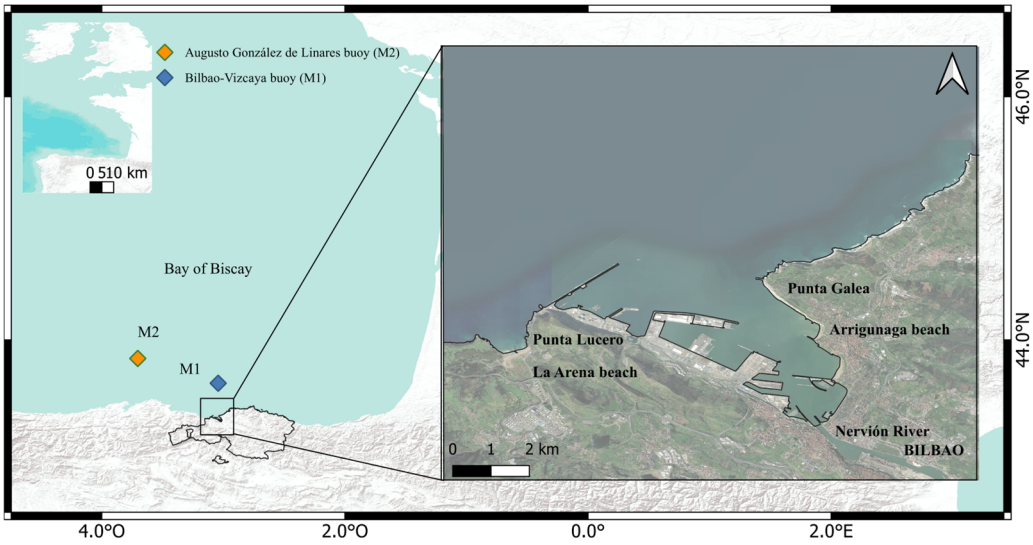


Figure 1. Location of the study area along the Bay of Biscay. The regional map provides geographical context within the northeastern Atlantic, while the enlarged panel shows the position of the offshore wave buoys used in this study.

The north-north-west (N-NW) orientation of the coastline and the absence of continental landmasses in that direction provide a practically unlimited fetch for waves generated in the North Atlantic. This configuration exposes the coast directly to wind fields associated with extratropical depressions crossing the ocean from west to east, with no significant sheltering or large-scale refraction effects before reaching the continental shelf.

2.2. Maritime Climate and Hydrodynamics

The local hydrodynamic regime is highly energetic and dominated by the following forcings:

- Wave climate: The wave climate is markedly directional, with a predominance of components from the W-NW sector. The annual mean significant wave height (H_S) ranges between 1.5 and 2 m. Statistical analyses indicate that H_S exceeds 3 m for more than 8% of the time in an average year, increasing to 29% during winter months [28]. During extreme winter events, H_S values exceeding 7–8 m are recorded, with T_P reaching 16–18 s [29].
- Tide and sea level: The area is classified as meso-tidal with a semidiurnal regime. The astronomical tidal range varies from 1 m during neap tides to 4.8 m during equinoctial spring tides. Additionally, the passage of deep low-pressure systems generates storm

surges that elevate the mean sea level, increasing the risk of coastal impact during high tides [28].

Consequently, the Bay of Biscay represents a particularly suitable natural laboratory for the analysis of extreme wave climate. Its direct exposure to North Atlantic storm tracks results in recurrent energetic wave conditions, allowing for statistically robust characterization of extreme events. Such environments provide valuable insights into the physical mechanisms governing storm generation and wave evolution and may serve as a reference framework for less energetic coastal regions where storm events occur less frequently but can still produce comparable impacts.

2.3. Coastal Morphology and Anthropogenic Context

Wave propagation towards the coast is strongly modulated by complex topography (Figure 1). The presence of rocky headlands (e.g., Punta Galea, Punta Lucero) and shallow shoals induces diffraction and refraction processes that filter wave energy unevenly along the coast. Recent studies [9] point out that exposed beaches such as La Arena receive incident waves with higher energy, whereas inner areas of the Abra (e.g., Arrigunaga) receive more attenuated and transformed wave spectra due to the protection offered by natural morphology and port structures.

The area hosts the Bilbao harbor, a key logistical infrastructure in the South-European Atlantic, located in the Outer Abra. Its sheltering structures, including the Punta Lucero breakwater and the Central Breakwater, are designed to operate under the severe Cantabrian maritime climate. Furthermore, the management of the adjacent beaches, which are of high tourist value, depends critically on wave variability, which controls erosive processes and safety in the bathing zone [30].

3. Materials and Methods

3.1. Wave and Climate Data

The analysis is based on in situ wave measurements obtained from two directional offshore deep-water buoys located along the Bay of Biscay (Figure 1 and Table 1). The primary dataset corresponds to the Bilbao-Vizcaya buoy (M1), which provides a long-term record spanning more than three decades and constitutes the main basis for extreme value analysis and trend detection [9]. The sampling frequency covers 3-hourly between 1990 and 2002 and hourly from 2002 onwards, resulting in a dataset of 175,190 observations, with 99,286 missing values (36.17%). Although the proportion of missing data is relatively high, no gap-filling or homogenization was applied in order to avoid introducing artificial variability, particularly in the analysis of extremes. In addition, the use of monthly aggregation and event-based approaches reduces the sensitivity of the analysis to short-term discontinuities in the record.

This buoy is moored at a depth of 600 m, beyond the influence of coastal bathymetry, and is therefore representative of offshore wave conditions directly associated with North Atlantic storm activity [31], ensuring that recorded wave heights reflect fully developed wave conditions.

To assess the sensitivity of detected trends to record length and temporal coverage, a second nearby offshore buoy, the Augusto González de Linares Oceanographic and Meteorological buoy (M2), is also considered. Although this record is substantially shorter, the M2 dataset has an hourly temporal resolution and was subjected to the same quality control procedures. It comprises 87,857 observations, with 13,031 missing values, corresponding to approximately 13% of the dataset.

The M1 dataset was obtained from the deep water buoy network (REDEXT) from Puertos del Estado (PdE) open access repositories, while the M2 dataset was provided under an

institutional agreement with the Instituto Español de Oceanografía (IEO). Both datasets correspond to quality-controlled observations, for which standard procedures (e.g., consistency checks and removal of erroneous values) were applied by the data providers prior to distribution. Therefore, no additional filtering was performed in this study.

Although both buoys are located in deep-water conditions, differences in water depth (600 m for M1 and 2850 m for M2) and offshore exposure may influence wave characteristics, particularly for long-period swell. Therefore, part of the observed differences between the two records may reflect spatial variability rather than record length alone.

The wave parameters analyzed in this study include H_S, T_P, and S (obtained as the ratio between H_S and the wavelength L [32]), which are commonly used wave descriptors in coastal engineering applications and extreme wave analysis [23,33]. Given that both buoys are located in deep offshore waters, the wavelength was estimated assuming deep-water conditions, using the linear wave theory approximation given in Equation (1), which is valid when the relative water depth is sufficiently large [34]. Consequently, wave steepness is derived under the deep-water assumption.

$$L = \frac{g \cdot T_P^2}{2\pi} \quad (1)$$

where g denotes gravitational acceleration.

The use of these two buoy records (Table 1) allows for a direct evaluation of the impact of record duration on statistics and trend estimations.

Table 1. Summary of the offshore wave datasets used in this study, including locations, water depth, and period analysis.

Buoy Name	Location	Water Depth [m]	Period Analyzed	Parameters	Sampling Interval
M1	(43°38′24″ N, 03°02′2″ W)	600	1990–2022	H_S, T_P, S, Storm metrics	3 h (1990–2002) 1 h (2002–2022)
M2	(43°50′40.20″ N, 03°46′12″ W)	2850	2007–2018	H_S, T_P, S, Storm metrics	1 h

The influence of large-scale atmospheric variability on wave climate and storm conditions along the Bay of Biscay was investigated using established climate circulation indices representative of North Atlantic atmospheric dynamics. In particular, the NAO and EA indices were selected due to their well-documented impacts on wind and pressure fields, storm tracks, and wave generation over the Atlantic [35–37]. Monthly values of the NAO, EA, and ENSO indices were obtained from the NOAA Climate Prediction Center's open teleconnection indices database and Physical Sciences Laboratory portal, covering the full period of wave observations analyzed in this study [38,39] (Figure 2). These indices were selected because they capture dominant modes of atmospheric variability that modulate the frequency, intensity, and trajectories of extratropical cyclones affecting the Bay of Biscay [40].

3.2. Extreme Event Definition

Extreme wave conditions were identified using a peak-over-threshold (POT) method, widely adopted in coastal engineering for the analysis of wave climate extremes (e.g., [9,41,42]). This method enables an efficient use of exceedances, providing a more robust characterization of extreme conditions compared to block maxima approaches, particularly when long-term records are available [43].

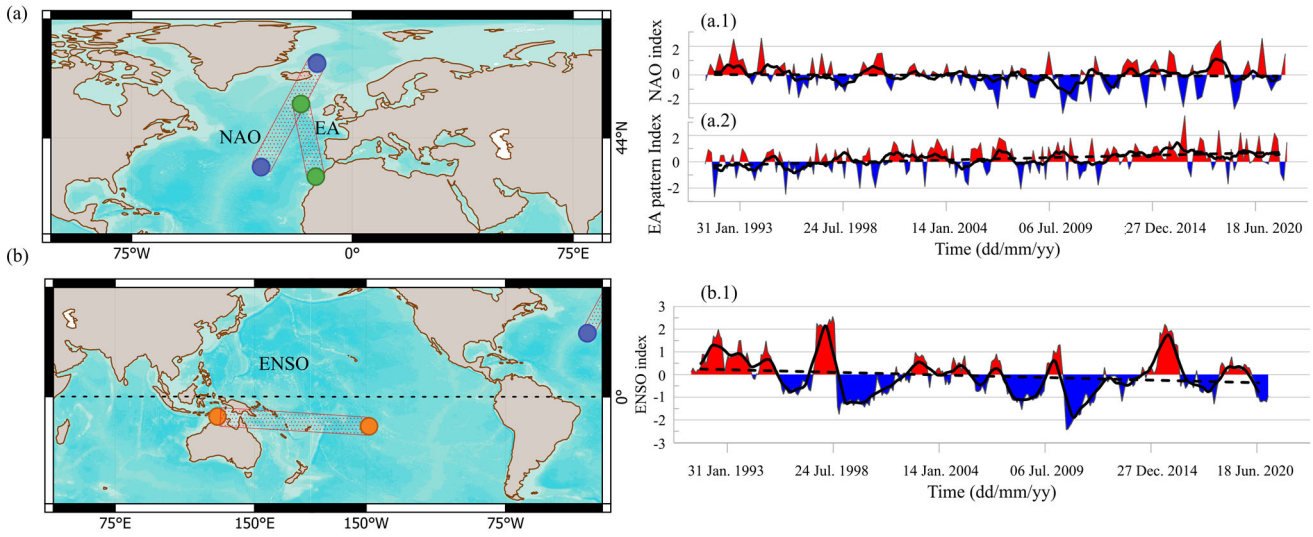


Figure 2. Spatial patterns and temporal variability in the large-scale climate indices considered in this study. Panels (**a**,**b**) illustrate the typical spatial influence of the NAO, EA, and ENSO index, highlighting the regional and remote nature of their associated atmospheric forcing. The blue, green, and orange markers indicate the representative centers of action associated with the NAO, EA, and ENSO, respectively, and the time series on the right show the temporal evolution of those indices ((**a.1**,**a.2**) for both NAO and EA index and (**b.1**) for ENSO) over the study period, with positive (red) and negative (blue) phases indicated.

The selection of the threshold (u) follows standard practice in extreme value analysis, where u is supported by mean residual life (MRL) plots (see Figure S1 in Supplementary Material), and selected as a compromise between retaining a sufficient number of extreme events and ensuring statistical independence and stability of parameter estimates. Previous studies suggest that, for relatively short records, avoiding excessively high thresholds and retaining enough exceedances is acceptable and may be required to improve the robustness of extreme value statistics, if independence criteria are satisfied (e.g., [44,45]).

In this study, a threshold value of u = 4.5 m for M1 and u = 3.9 m for M2 was selected based on a combined assessment of event independence, sample size, and stability of return level estimates. Although the Akaike Information Criteria (AIC) and its small-sample correction (AICc) were evaluated and used as complementary tools to guide threshold selection and generally improved as the threshold increased, substantially higher thresholds led to a marked reduction in the number of exceedances. This leads to less stable return level estimates and wider confidence intervals at long return periods.

To ensure statistical robustness, a minimum of 5 h duration and a minimum temporal separation of 120 h was imposed between peaks exceeding the threshold according to the specific Puertos del Estado (PdE) assessment [46]. Different events with a time separation shorter than 120 h were considered part of the same extreme episode and represented by the maximum significant wave height recorded during that period. For each identified extreme event, associated wave parameters were extracted, including H_S, T_P, and S.

3.2.1. Sensitivity of Threshold Selection

To evaluate the robustness of the selected thresholds for both buoy records (u = 4.5 m for M1 and u = 3.9 m for M2), additional sensitivity analyses were conducted by testing alternative thresholds within ± 0.5 m under the same declustering window (120 h). For each tested threshold, the number of independent exceedances was identified for both records over the analyzed period, corresponding to an average rate of events per year (λ) and the 50-year return levels were estimated. This procedure was designed to assess the stability of

extreme value inference and to ensure that the selected thresholds provided a statistically robust compromise between sample size and tail representativeness, particularly in the case of the shorter M2 record.

3.2.2. Extreme Value Modelling

Exceedances over the selected threshold were modelled using a Generalized Pareto Distribution (GPD), estimated using maximum likelihood estimation (MLE) consistent with the asymptotic formulation of the POT framework [47–49]. If u denotes the selected threshold and the exceedances are defined as in Equation (2):

$$y = H_S - u,\ y \geq 0 \tag{2}$$

It was assumed that the exceedances follow a GPD with a cumulative distribution function given by Equation (3):

$$G(y) = 1 - \left[1 + k\left(\frac{y}{\beta}\right)\right]^{-1/k}, k \neq 0 \tag{3}$$

where $\beta > 0$ is the scale parameter, and k is the shape parameter controlling the tail behavior. The return levels were then expressed in terms of the original variable H_S by adding the threshold u. The domain of validity of Equation (3) is [44]:

$$y \geq 0, 1 + k\frac{y}{\beta} > 0 \tag{4}$$

3.3. Storm Characterization

Storm (extreme) events were described in Section 3.2. For each identified storm, a set of representative parameters was extracted to characterize storm intensity and temporal evolution. These parameters include the maximum significant wave height reached during the storm and the associated peak period. Wave steepness was also considered according to Equation (1) and aggregated at a monthly scale to analyze long-term variability and trends in storm activity along the Bay of Biscay [50]. Monthly aggregation was adopted to reduce the influence of short-term persistence while preserving sensitivity to interannual and longer-term variability. The storm identification and characterization procedure are illustrated in Figure 3, which shows the application of the threshold-based approach to the significant wave height time series for both buoy records.

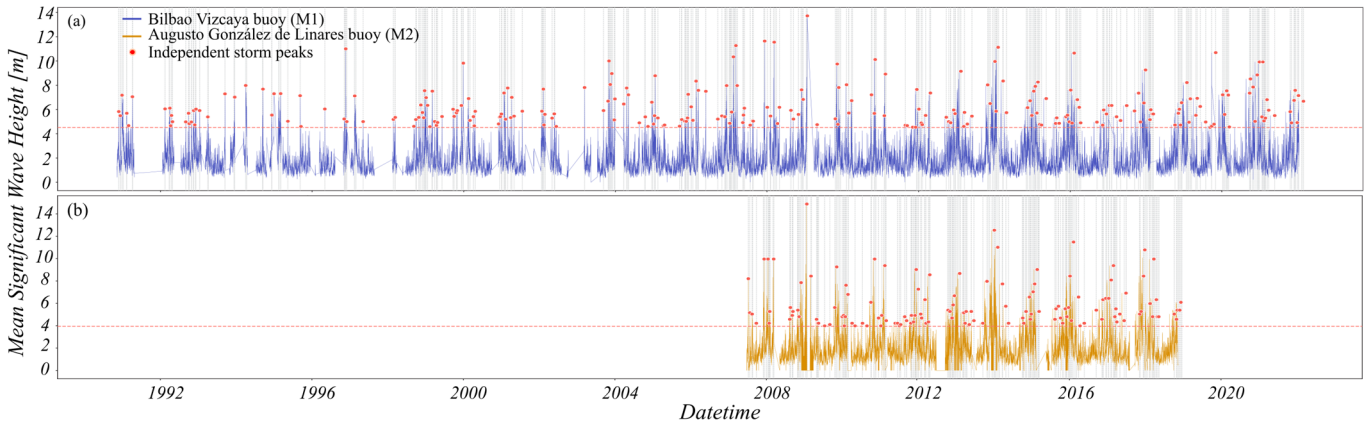


Figure 3. Illustration of the storm identification procedure based on the POT method applied to significant wave height time series from (**a**) the Bilbao-Vizcaya buoy (M1) and (**b**) the Augusto González de Linares buoy. The horizontal dashed line indicates the selected threshold, while red markers identify independent extreme events.

3.4. Trend Analysis

Trends in monthly aggregated extreme wave and storm-related parameters were assessed using the non-parametric Mann–Kendall (MK) test, which is widely applied in hydro-meteorological studies due to its robustness to non-normal data distributions, outliers, and non-linear variability [51,52]. This test evaluates the presence of monotonic trends using Sen's slope as an estimator parameter to quantify the median rate of change, as it is less sensitive to extreme values than parametric regression approaches, with statistical significance evaluated at the 95% confidence level [53]. Prior to trend analysis, wave time series were aggregated to monthly values. This aggregation was adopted to reduce the influence of short-term variability and serial dependence inherent in hydrodynamic data, which can artificially inflate the significance of trend tests if not properly accounted for [54]. Preliminary analyses indicated the presence of pronounced autocorrelation at weekly time scales.

Monthly aggregation provides an effective compromise between mitigating the effects of autocorrelation and retaining sensitivity to interannual and longer-term variability. This effect is confirmed by the autocorrelation analysis (see Table S1 in the Supplementary Material), where lag-1 autocorrelation coefficients range between approximately -0.48 and 0.28, depending on the parameter and dataset. At a monthly resolution, autocorrelation coefficients decrease rapidly with increasing lag, and values beyond the first lag are generally small, indicating a limited influence of serial dependence on the MK test results. Similar aggregation strategies have been adopted in previous wave climate trend studies to improve the robustness of non-parametric trend estimates, demonstrating that autocorrelation coefficients along the lags decrease rapidly after lag 0 [9,54,55].

To further ensure the robustness of trend inference under residual serial correlation, trend significance was additionally evaluated using MK tests that account for autocorrelation in the data, with the Yue–Wang (YW) [56] and Hamed-Rao (HR) [57] modifications applied as complementary diagnostics. For the storm analysis, an annual aggregation scale was adopted to avoid serial correlation in storm counts and annual storm wave power prior to trend detection. Lag-1 autocorrelation coefficients are generally low to moderate (see Table S1), and Ljung–Box tests do not reject the null hypothesis of no serial correlation ($p > 0.05$), with similar patterns observed for the shorter M2 record; therefore, classical MK tests were considered adequate for annual storm metrics.

Having established the suitability of these non-parametric approaches for detecting trends, linear models were also fitted to the annual storm metrics to provide a complementary parametric representation and clearer visualization of the tendencies. Since these annual values represent aggregated counts, within-trial error bars (e.g., standard deviations) are not applicable, and the associated uncertainty in the parametric trends is instead expressed through 95% confidence intervals derived from the regression models.

3.5. Atmospheric Circulation Indices

To examine potential relationships between atmospheric circulation patterns and wave-related parameters, correlations and lagged cross-correlation analyses were performed between the climate indices and wave variables. Lagged Pearson's correlations were considered to account for delayed oceanic responses to atmospheric forcing, which may arise from storm development, wave development, and swell propagation processes. Both synchronous and lagged relationships were explored and obtained using Equation (5) to identify the temporal scales at which atmospheric variability exerts the strongest influence [9].

$$r_{X_1X_2}(k) = \frac{\sum_{t=1}^{N-k} \left(X_1(t) - \overline{X_1}\right)\left(X_2(t+k) - \overline{X_2}\right)}{\sqrt{\sum_{t=1}^{N-k} \left(X_1(t) - \overline{X_1}\right)^2 \sum_{t=1}^{N-k} \left(X_2(t+k) - \overline{X_2}\right)^2}} \quad (5)$$

where X_1 (t) and X_2 (t) represent the monthly time series of wave parameters and climate indices, respectively, k is the lag (in months), and N is the length of the series [58].

All correlation analyses were conducted using monthly aggregated time series to ensure consistency with the trend analysis framework (see Section 3.4). In addition, a multiple linear regression model was fitted to monthly H_S as a linear additive function of the selected climate indices. Model parameters were estimated by ordinary least squares using months with complete data. The coefficient of determination (R^2) was used as a compact measure of the proportion of sample variance in monthly H_S explained by the predictors [59].

4. Results

4.1. Extreme Wave Climate and Return Levels

Extreme wave analysis was applied to significant wave height records from offshore locations (see Table 1) to characterize the extreme wave climate along the Bay of Biscay. The careful selection of the thresholds ensures that a sufficient number of independent exceedances is obtained, thereby supporting the statistical robustness of the POT framework.

For the M1 record, the threshold (u = 4.5 m) yields 263 independent exceedances over the analyzed period, corresponding to an average rate of approximately 8.2 events per year. In contrast, for the shorter M2 record, the threshold (u = 3.9 m) results in 132 independent exceedances, corresponding to approximately 11 events per year.

This selection of exceedances provides a statistically robust basis for estimating return levels, as illustrated in Figure 4 for the M1 and M2 buoys, together with the corresponding 90% CIs derived from the fitted extreme value models.

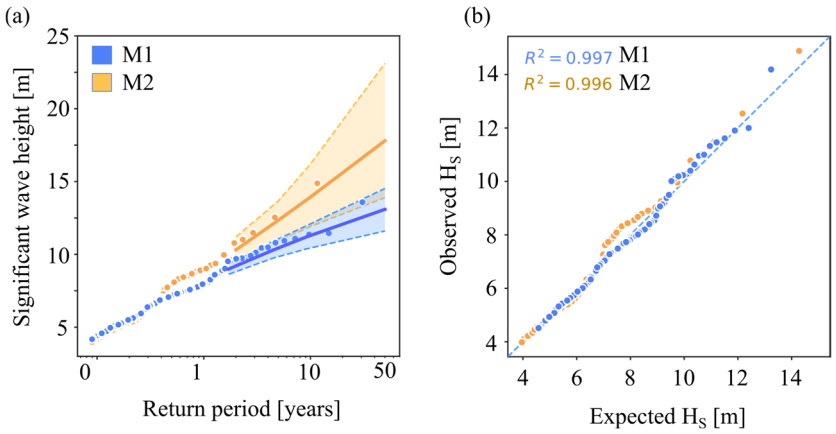


Figure 4. Return level plot of significant wave height as a function of return period, derived from the fitted GPD model at the Bilbao-Vizcaya (M1) and Augusto González de Linares (M2) buoys. (**a**) Estimated return levels of significant wave height as a function of return period, including 90% confidence intervals. (**b**) Quantile-Quantile (QQ) plots comparing observed and theoretical extreme significant wave height values for both buoy records.

The return level curves indicate higher estimated extreme wave heights at the M2 record compared to M1 for the same return period. However, uncertainty bands increase markedly with return period for the M2 dataset, reflecting the substantially shorter length of the observational record relative to the long-term M1 buoy. These wider uncertainty bounds should be interpreted primarily as an effect of limited temporal coverage, whereas differences in return-level magnitude may also reflect the greater offshore exposure and deeper-water location of M2.

To further quantify the uncertainty associated with the estimated return levels, the relative width of the confidence intervals was computed as the difference between the

upper and lower confidence limits normalized by the central estimate (Table 2). The results show that relative uncertainty increases with the return period for both datasets but is consistently higher for the M2 records. For instance, relative uncertainty values of 14.75% and 20.48% are obtained for the 10-year and 50-year return periods at M1, whereas corresponding values for M2 are 37.32% and 50.31%, respectively.

Table 2. Estimated return levels of significant wave height for selected return periods at the M1 and M2 buoys. Upper and lower confidence limits are reported together with the relative width of the confidence interval, expressed as a percentage of the central return level estimate, to quantify the uncertainty associated with the record length.

Return Period [Years]	Estimated Value	$H_{S,M1}$ [m]	Relative M1 Uncertainty [%]	$H_{S,M2}$ [m]	Relative M2 Uncertainty [%]
Tr = 10 years	Upper limit	12.22	14.75	16.97	37.20
	Central value	11.46		14.23	
	Lower limit	10.53		11.66	
Tr = 50 years	Upper limit	14.59	20.48	23.19	50.31
	Central value	13.24		17.81	
	Lower limit	11.88		14.23	

Differences between the two datasets not only reflect the influence of record length but also variations in exposure and observational characteristics. The M2 buoy, deployed in deeper water and further offshore (see Table 1), likely contributes to the higher estimated return levels. In contrast, the longer and more continuous M1 record provides more constrained estimates, particularly for long return periods. It should be noted that the threshold selected for the extreme value analysis differs slightly between buoys. While this choice ensures an adequate number of independent extreme events and improves the statistical robustness of each dataset, it may also limit the direct comparability of return level estimates between M1 and M2, and should therefore be considered when interpreting differences between records.

To explicitly assess the sensitivity of the extreme value estimates to threshold selection, a threshold calibration analysis was performed (see Section 3.2.1). For the long-term M1 record, the return level at 50 years (RL50) remains highly stable across the tested thresholds. Varying the threshold within ± 0.5 m around the adopted value results in RL50 estimates ranging from 13.37 m to 13.39 m, corresponding to relative changes of approximately +0.96% to +1.14% relative to the reference estimate (13.24 m), confirming the robustness of the selected threshold. For the shorter M2 record, the estimated 50-year return level exhibits a more pronounced dependence on the selected threshold. RL50 estimates range from 16.60 m (u = 3.4 m) to 18.28 m (u = 4.4 m), corresponding to changes of approximately -6.8% to +2.7% relative to the reference estimate (17.81 m). Although the magnitude of this variation remains moderate, it illustrates the greater structural sensitivity of extreme value inference when derived from shorter observational records, which is consistent with the higher variability observed in the threshold diagnostics (see Figure S1 in the Supplementary Material).

4.2. Storm Characteristics and Variability

Storm events identified using the POT approach (see Section 3.2) were evaluated separately for the M1 and M2 buoy records to account for differences in record length and observational settings (Figure 3). The analysis reveals marked temporal variability in storm occurrence and intensity at both locations. Storm frequency exhibits strong interannual variability, with periods of enhanced storm activity alternating with comparatively calmer

intervals. Despite these fluctuations, both buoy records show a broadly consistent pattern in the timing of stormy periods.

Storm intensity, quantified by the maximum significant wave height recorded during each storm, is generally higher at the M2 station than at M1 (Figure 3). This difference is consistent with the deeper water deployment and greater offshore exposure of the M2 location. However, the shorter duration of the M2 record results in increased variability and uncertainty in the statistical representation of extreme storm characteristics, particularly for the most energetic events.

4.3. Trends in Monthly Wave Parameters

For the long-term M1 record (Table 3), no statistically significant trend is detected in the monthly averaged significant wave height at the 95% confidence interval. The estimated Sen slope indicates a positive trend, with magnitudes on the order of a few millimeters per year. In contrast, the peak period exhibits a statistically significant decreasing trend consistently identified using both the standard and seasonal MK tests. Therefore, wave steepness shows a statistically significant increasing trend ($S = +3.8 \cdot 10^{-5}$ month^{-1}, $p < 0.05$), indicating structural changes in wave steepness.

Table 3. Summary of trend estimations for wave parameters derived from the MK test and Sen's slope estimator for the M1 and M2 buoys. Trends are evaluated at the 95% confidence level using monthly aggregated values. The *p*-values reported under YW and HR correspond to the modified MK tests, respectively, applied to account for serial correlation.

Buoy	Parameter	Sen Slope	*p*-Value (MK)	*p*-Value (YW/HR)
M1	H_S	$+2.2 \cdot 10^{-4}$ m·month^{-1}	0.503	0.189/0.189
	T_P	$-4.0 \cdot 10^{-3}$ s·month^{-1}	<0.001 *	<0.001 */<0.001 *
	Steepness	$+3.8 \cdot 10^{-5}$ month^{-1}	<0.001 *	<0.001 */<0.001 *
M2	H_S	$+2.0 \cdot 10^{-3}$ m·month^{-1}	0.328	<0.001 */0.27
	T_P	$+4.0 \cdot 10^{-3}$ s·month^{-1}	0.220	<0.001 */0.13
	Steepness	$-3.2 \cdot 10^{-7}$ month^{-1}	0.619	0.12/0.70

* Indicate a statistically significant result.

Trend estimates derived from the shorter M2 record are not statistically significant for any of the wave parameters. For this shorter record, no statistically significant trends are detected in monthly significant H_S, T_P, and S at the 95% confidence level. The estimated Sen slopes are small and exhibit higher variability, reflecting the strong influence of interannual fluctuations and the limited temporal coverage available for robust trend detection.

Modified MK tests for M1, accounting for serial correlation, yielded consistent trend directions and significance levels with respect to the classical MK test (Table 3), supporting the robustness of the detected trends. In contrast, assessing trend significance for the M2 record requires additional caution. For this shorter series, the modified MK tests produce inconsistent significance levels depending on the chosen autocorrelation correction. While the YW adjustment suggests statistically significant trends in H_S and T_P, neither the classical MK test nor the HR modification confirms these findings.

This inconsistency in M2 arises despite relatively low lag-1 autocorrelation (Table S1 in the Supplementary Material), indicating that the discrepancies are not driven by strong serial dependence but rather by the sensitivity of significance estimates to the selected correction method under limited sample size. Therefore, trend significance in M2 should be interpreted with caution.

4.4. Trends in Storm Occurrence and Intensity

Storm trends were analyzed, focusing on interannual variations in storm occurrence and associated storm energy. This complements the monthly wave assessment by explicitly characterizing storm activity and its temporal variability. Figure 5 illustrates the temporal evolution of storm activity along the Bay of Biscay derived from the offshore buoy records. Linear trends and their associated 95% CI are included to illustrate the uncertainty in the temporal evolution.

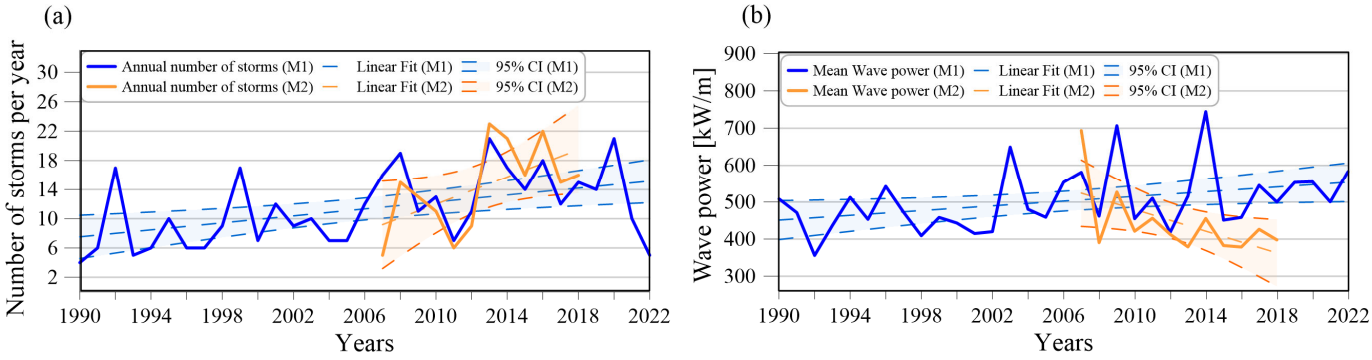


Figure 5. Temporal evolution of storm activity along the Bay of Biscay derived from both offshore buoy records, showing (**a**) the annual number of identified storm events and (**b**) the associated annual storm wave power. Solid lines represent annual values, dashed lines indicate linear trends, and shaded areas correspond to the 95% confidence intervals of the fitted regressions.

The M1 dataset shows pronounced interannual variability in both the annual number of storm events (Figure 5a) and the associated storm wave power (Figure 5b). Periods of enhanced storm frequency are interspersed with comparatively lower calmer intervals, as seen during 1990–1998 and 2015–2022, and years with elevated storm energy do not always coincide with peaks in storm occurrence.

Quantitative trend estimates derived from the MK test and Sen's slope estimator are summarized in Table 4. For the M1 buoy, statistically significant positive trends are detected in both the annual number of storms and storm wave power at 95% confidence level. The estimated Sen slopes (e.g., +0.28 storms·year^{-1} and +2.90 kW·year^{-1}, respectively) indicate a gradual increase in storm frequency (equivalent to approximately nine additional storm events over the 32-year period) accompanied by a concurrent rise in storm power.

Table 4. Trend estimators in storm occurrence and storm energy derived from the MK test and Sen slope estimator.

Parameter	Buoy	Sen Slope	*p*-Value (MK)
Annual No. of storms	M1	+0.28 storms·year^{-1}	<0.001 *
Storm Wave power		+2.90 kW·year^{-1}	0.017 *
Annual No. of storms	M2	+0.96 storms·year^{-1}	0.001 *
Storm Wave power		−8.42 kW·year^{-1}	0.086

* Indicate a statistically significant result.

Results obtained from the shorter M2 record differ from those observed at M1. While a statistically significant trend is identified for annual frequency, no significant trend is detected in the storm wave power (p-value > 0.05). Trend estimates for M2 exhibit greater variability and sensitivity to individual years due to the limited temporal coverage of the dataset.

4.5. Influence of Large-Scale Climate Indices on Wave Parameters

The influence of large-scale climate variability on wave conditions along the Bay of Biscay was assessed by using Equation (5) (see Section 3.5) in which a cross-correlation analysis is conducted between climate indices and wave parameters derived from the two buoy records. The use of different climate indices (e.g., NAO, EA, and ENSO) allows for a good estimation of which atmospheric modes might play a role in modulating ocean variability (Figure 6).

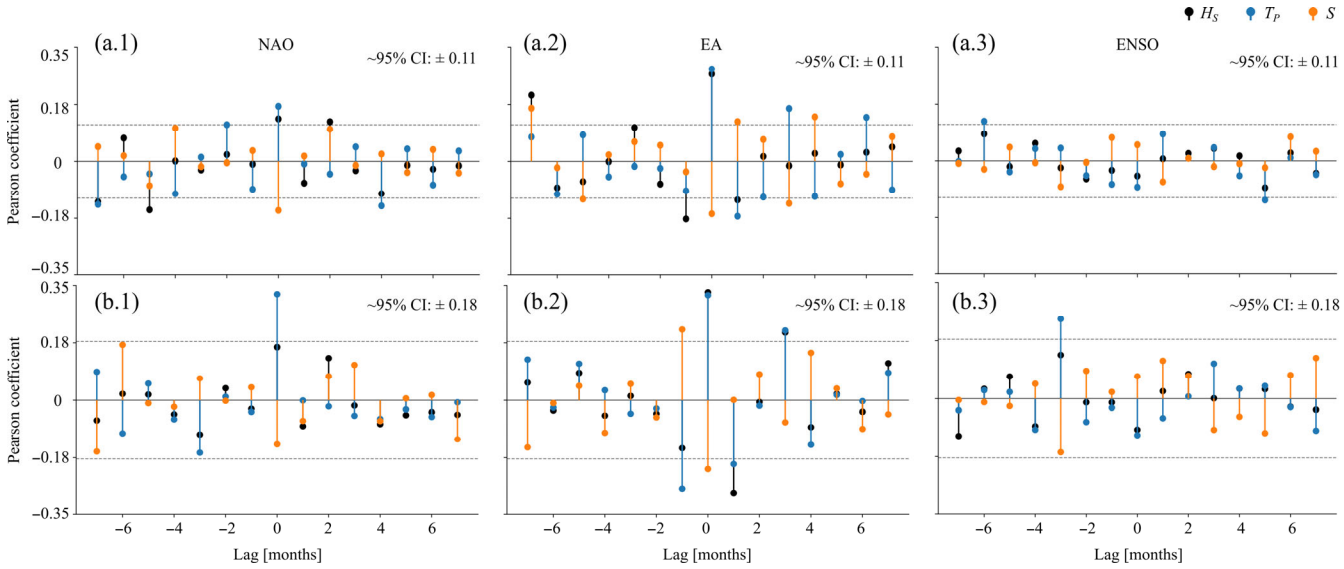


Figure 6. Lagged Pearson's correlation coefficients between large-scale climate indices (NAO, EA, and ENSO) and monthly wave parameters derived from the offshore buoy records. Correlations are shown as a function of lag (months) for significant H_S, T_P, and S. Dashed horizontal lines indicate the 95% confidence interval for statistical significance. The results are presented separately for the long-term M1 record (**a.1**–**a.3**) and the shorter M2 record (**b.1**–**b.3**), corresponding to NAO, EA and ENSO, respectively.

At lag zero (synchronous correlation), statistically significant correlations are identified between North Atlantic atmospheric indices and wave parameters for the M1 long-term record. Both NAO and EA patterns exhibit weak to moderate correlations with significant wave height and peak period, with EA consistently showing a stronger relation (Figure 6(a.1,a.2)). Pearson's correlation coefficients for EA reach values of approximately 0.27 for H_S and 0.28 for T_P, whereas NAO correlations are weaker, with coefficients on the order of 0.13–0.17. Wave steepness is negatively correlated with both indices, indicating a tendency toward less steep waves under positive phases of NAO and EA.

Correlation patterns derived from the shorter M2 buoy are generally consistent in sign with those obtained for M1, although correlation magnitudes are in some cases higher. For M2, statistically significant correlations are observed between the EA index and both significant wave height and peak period, with coefficients exceeding 0.3 at lag zero (Figure 6(b.1,b.2), and Table 5). NAO exhibits a significant relation with peak period, while correlations with significant wave height and wave steepness remain statistically insignificant (p-value > 0.05). These differences reflect the reduced temporal coverage of the M2 records and the associated increase in uncertainty regarding extreme wave statistics (Figure 4).

In contrast, no statistically significant simultaneous correlations are detected between ENSO and any of the analyzed wave parameters at either buoy location (Figure 6(a.3,b.3) and Table 5). Correlation coefficients at lag zero are small in magnitude, indicating the absence of a direct simultaneous relation between ENSO variability and wave conditions

in the Cantabrian Sea. However, cross-correlation analysis reveals weak but statistically significant delayed correlations between ENSO and wave parameters with maximum correlation values on the order of 0.10–0.15 occurring at lags of approximately six months. This behavior indicates a time-lagged and indirect weak influence of ENSO on regional wave characteristics.

Table 5. Correlation between large-scale climate indices and wave parameters for M1 and M2 at lag zero.

Index	Parameter	r (M1)	*p*-Value	r (M2)	*p*-Value
NAO	H_S	+0.13	0.029 *	+0.162	0.086
	T_P	+0.17	0.003 *	+0.32	<0.001 *
	S	−0.15	0.009 *	−0.16	0.085
EA	H_S	+0.27	<0.001 *	+0.340	<0.001 *
	T_P	+0.28	<0.001 *	+0.340	<0.001 *
	S	−0.16	0.005 *	−0.260	0.004 *
ENSO	H_S	−0.05	0.429	−0.09	0.321
	T_P	−0.08	0.166	−0.07	0.438
	S	+0.05	0.390	+0.03	0.779

* Indicate a statistically significant result.

To further evaluate the combined influence of the atmospheric modes, the results of the multiple linear regression analysis (see Section 3.5), show for the longer term M1 record, the three indices jointly explain approximately 8.6% of the total variance, with NAO an EA remaining statistically significant predictors, whereas ENSO does not contribute significantly. A similar result is obtained for M2, where the explained variance is approximately 7.4%.

5. Discussion

5.1. Comparison with Previous Wave Climate Studies in the Bay of Biscay and the North Atlantic

The consistency of these results with previous studies reinforces the interpretation that apparent discrepancies in reported wave trends across the Bay of Biscay are largely driven by methodological choices and record length dependencies rather than reflecting fundamentally different physical mechanisms. Several studies have reported positive trends in significant wave height, emphasizing the dominant role of strong variability in this region (e.g., [60–62]). Where positive trends in significant wave height have been identified, their magnitude and statistical significance have often been shown to depend strongly on the analyzed period, the data source, and the length of the available observational record [63,64]. This sensitivity has been repeatedly highlighted as a key limitation for the detection of long-term changes in wave conditions.

In this context, and after accounting for residual serial correlation through modified MK tests, the lack of a statistically significant trend in monthly H_S values identified for the long record (M1 buoy) is consistent with most of the existing literature for the Bay of Biscay and adjacent North Atlantic regions [14,15]. These findings indicate that the absence of a statistically significant trend in H_S does not imply stability of the extreme wave climate but rather suggests that structural changes may occur in storm frequency, wave peak period, and wave steepness that are not reflected in wave height.

In contrast, the statistically significant decrease in peak period detected in the M1 record (Table 3), together with the associated increase in wave steepness, suggests more subtle but potentially relevant changes in wave characteristics that are not captured by H_S alone. Similar behavior toward changes in wave period and spectral characteristics has been reported in previous studies for the Bay of Biscay and has been linked to shifts in

storm tracks, wind forcing, and the relative contribution of locally generated seas versus long and well-formed swell (e.g., [15]).

Lastly, the absence of statistically significant trends in the shorter M2 record (Table 3), together with its sensitivity to autocorrelation correction, further supports the strong dependence of statistical inference on record length. In particular, the discrepancy between the YW-adjusted results and those obtained with the classical MK and HR approaches for H_S and T_P indicates that the statistical significance of trends depends on the possible existence of serial dependence in consecutive data. Rather than providing robust evidence of monotonic change, these mixed results suggest limited inferential stability under short temporal coverage, where interannual variability and autocorrelation correction may substantially affect *p*-values [65,66]. This interpretation is further supported by the correlation between M1 and M2 wave parameters during the overlapping period (see Table S2 in Supplementary Material), indicating that both records reflect a coherent regional signal.

5.2. Implications of Record Length and Uncertainty in Extreme Wave Climate Assessment

The direct comparison between the long-term (M1) records and the shorter (M2) buoy demonstrates the structural dependence of extreme value inference on temporal coverage (see Figure 4). While both buoys are located in deep water and are influenced by similar large-scale atmospheric forcing, differences in offshore exposure and water depth also contribute to the contrasts observed between M1 and M2. In this context, the substantially shorter duration of the M2 dataset primarily affects the robustness and uncertainty of the extreme value estimates, rather than solely explaining their magnitude [67]. This contrast becomes even more apparent when examining how record length influences the uncertainty structure of the extreme value estimates.

Results from the extreme value analysis demonstrate that return level estimates derived from the M2 record are characterized by significantly wider confidence intervals, particularly for long return periods. This pattern, also reported in previous studies [24], is illustrated in Table 2, where relative uncertainty exceeds 30% for Tr = 10 years and approaches 50% for Tr = 50 years. In contrast, the longer M1 record yields more constrained confidence intervals, reflecting the stabilizing effect of extended record duration on extreme value inference. This indicates that the tail distribution becomes progressively unstable as record length decreases.

In addition to the widening confidence intervals observed for long return periods, the sensitivity of return level estimates to threshold selection further confirms that this sensitivity is amplified in short records, thereby conditioning design-level inference. While the longer records exhibit limited variation in RL50 under threshold selection, the shorter M2 records show a more pronounced response.

This pattern is consistent with the threshold diagnostics presented in Figure S1, where the mean residual life plot for the M1 dataset shows a relatively stable region across a range of thresholds, while the M2 dataset exhibits a greater variability. This reflects the increased sensitivity of threshold selection to sampling variability in shorter records and supports the interpretation that extreme value inference becomes structurally less robust as record length decreases.

From a coastal engineering perspective, these differences translate into fundamentally different design envelopes, potentially leading to either over-conservative or non-conservative safety margins depending on the record length considered. These results reinforce previous findings that caution against the direct use of short records for the derivation of long return period design conditions without explicit consideration of uncertainty [68,69].

5.3. Storminess Versus Wave Height: Implications for Coastal Engineering

The combined storm-based and parameter-based analysis reveals that long-term changes in extreme wave climate along the Bay of Biscay are more clearly expressed in storminess metrics and wave peak period than in significant wave height. While no statistically significant long-term trend is detected in monthly wave height for the M1 records, the storm-based analysis indicates a statistically significant increase in both the annual number of storm events and the associated storm wave power. This highlights the importance of distinguishing between mean wave height statistics and storminess metrics when assessing long-term changes [70].

An increase in storm frequency (see Figure 5a) without a corresponding statistical increase in wave height (see Table 3) suggests that changes in wave climate may be driven by a higher occurrence of moderately extreme storm events rather than by an intensification of the mean climate, which is also consistent with previous findings (e.g., [71]). Moreover, the observed increase in storm wave power for M1 (Figure 5b and Table 4) further supports this interpretation. Wave power integrates both H_S and T_P and is therefore more sensitive to changes in storm duration and spectral characteristics than wave height alone. This concurrent increase in storm wave power, the decrease in peak wave period, and the increase in wave steepness identified in the long-term record (see Tables 3 and 4) may indicate a propensity toward steeper wave conditions during storms. Such conditions may be associated with enhanced wave-induced loads on offshore and coastal structures and more frequent and severe impacts, as higher wave steepness has been shown to increase force responses on structural elements under wave attack [72].

From a physical perspective, these changes may be related to modifications in storm characteristics and atmospheric forcing over the North Atlantic. For instance, potential shifts in storm-track position or trajectories could result in storms occurring closer to the study area, reducing the effective fetch and limiting wave development, which would be consistent with shorter peak periods and increased steepness. Similarly, variations in storm duration or wind-field persistence may influence wave growth conditions, leading to less developed sea states. Changes in wind intensity or variability could further contribute to a relative increase in locally generated wind-sea conditions compared to long-period swell. However, these interpretations should be considered as plausible hypotheses, since the present analysis is based on bulk wave parameters and does not include spectral partitioning or wind-field data.

In contrast, results derived from the shorter M2 record show a greater variability and, in some cases, opposing trends (Figure 5b), highlighting the sensitivity of storminess metrics to record length [66]. Furthermore, storm metrics are inherently dependent on the selected POT threshold and declustering criteria. Although a consistent methodology was applied across both datasets, the shorter M2 record is more sensitive to threshold selection, as small variations in the threshold can significantly modify the number of identified events and their associated metrics. This sensitivity may partially explain the variability and the non-significant negative trend observed in storm wave power for M2, which should therefore be interpreted with caution as it may reflect sampling variability rather than a robust physical signal.

5.4. Relation Between Large-Scale Atmospheric Indices on Wave Variability

The influence of large-scale atmospheric circulation on wave variability in the study zone was further examined through complementary statistical analyses, including a correlation assessment (see Section 4.5). These analyses provide additional insight into the extent to which dominant climate modes modulate wave conditions and help contextualize the physically meaningful relationships identified in the results (Figure 6).

At monthly scales, correlation analysis indicates that the NAO index and the EA pattern exhibit statistically significant correlations with all wave parameters for the long-term record, particularly wave peak period. The dominance of T_P correlations, compared to those of significant wave height, indicates that large-scale atmospheric circulation primarily influences the spectral structure and energy distribution of the wave field rather than simply increasing wave heights. The strongest correlations occur at lag zero, suggesting a relatively rapid atmospheric control on wave characteristics associated with changes in wind strength, fetch, and storm-track orientation [73]. The persistence of significant correlations suggests that NAO and EA act as modulators of wave properties in the Bay of Biscay [74].

For the longer record (M1), the regression analysis (see Section 4.5) further confirms the combined influence of NAO and EA, which together explain approximately 8–9% of the monthly variability in the mean wave climate. This suggests that a substantial fraction of variability remains controlled by mesoscale processes and local dynamics. Although the proportion of explained variance is modest, it is consistent with previous studies in the northeast Atlantic and reflects the complex, multi-scale nature of wave generation processes [15,74,75]. Within this context, large-scale atmospheric modes should be interpreted as contributors that modulate the background variability and storminess of the wave climate, rather than as deterministic predictors of hydrodynamic conditions. The statistically significant regression coefficients nonetheless demonstrate that these modes exert a measurable and physically coherent influence on monthly wave variability, even when local and mesoscale processes dominate the overall variance [76].

Results derived from the shorter record (M2) exhibit more nuanced behavior. As shown in Figure 6(b.1,b.2), significant wave height does not display a statistically significant correlation with the NAO at the 95% confidence level, although correlation values at lag zero remain positive and close to the significance threshold. In contrast, the EA pattern shows a statistically significant relation with H_S, as well as with the peak period.

As M2 results follow the same trend in terms of correlation, the reduced statistical significance of the NAO with the H_S at M2 is interpreted as a combined effect of record length limitations and enhanced interannual variability (Table 5), rather than as a fundamentally different physical response. As shown in previous results, short observational records are more sensitive to individual storm seasons and episodic events, which can obscure otherwise robust climate-wave relations. This interpretation is consistent with the higher variability and reduced stability of the extreme assessment (see Section 4.1), and the correlation coefficients observed for M2 across different lags (Figure 6(b.1-b.3) & Table 5).

In contrast to the NAO and EA indices, the influence of ENSO on wave variability along the Bay of Biscay appears to be weaker and largely indirect. At lag zero, ENSO does not show statistically significant correlations with any of the analyzed wave parameters at either buoy location, indicating the absence of a direct simultaneous relation with regional wave forcing (Figure 6). However, the lagged cross-correlation analysis reveals weak but statistically significant delayed relations, particularly for peak period, with maximum correlation values below 0.15 at lags of about 3 to 6 months.

This delayed signal is consistent with mechanisms proposed in the literature whereby ENSO may affect North Atlantic climate through remote pathways. One possible pathway is a tropospheric Rossby-wave response extending from the tropical Pacific across the Pacific–North American sector and projecting onto North Atlantic circulation [77]. Another is an indirect pathway through lagged sea surface temperature anomalies in the tropical North Atlantic, arising through an atmospheric bridge involving changes in trade winds, evaporation, and large-scale tropical Atlantic circulation [78,79]. Through these large-scale adjustments, ENSO may indirectly modulate the atmospheric conditions

that influence North Atlantic storm-track behavior and, ultimately, wave generation at mid-latitudes [80,81].

However, these mechanisms are not directly resolved in the present study, since our analysis is based on statistical relationships between monthly climate indices and wave parameters and does not include atmospheric reanalysis, storm-track diagnostics, or sea surface temperature fields. Therefore, the ENSO signal reported here should be interpreted cautiously as a weak statistical association consistent with previously proposed remote teleconnection pathways, rather than as demonstrated causal attribution.

Overall, the combined results highlight that extreme wave climate variability along the Bay of Biscay cannot be adequately characterized using significant wave height alone. Structural changes in storm frequency, peak period, and wave steepness may occur without manifesting as statistically significant trends in H_S. Furthermore, the direct comparison between long and short observational records demonstrates that trend detection and extreme value inference remain structurally sensitive to record length. These findings also have relevant practical implications for coastal engineering and management, as discussed in the following section.

5.5. Practical Implications for Coastal Engineering and Management

The results obtained in this study have several practical implications for coastal engineering and management. From an operational perspective, the observed increase in storm frequency and storm wave power identified in the longer dataset has direct relevance for port operations and safety in the Bilbao harbor. More frequent storm events and steeper wave conditions may affect operational and navigation safety, and impose additional loads on port infrastructure, particularly during extreme winter conditions.

In addition, the identified trends in S and T_P highlight the importance of considering changes in wave spectral characteristics, rather than relying exclusively on H_S. These changes may also have direct implications for coastal risk management, particularly in terms of erosion processes, coastal flooding, and infrastructure vulnerability [82].

Beyond these engineering applications, wave climate variability also plays a key role in surf tourism. Previous studies demonstrate how wave conditions can be used to characterize tourism seasonality, beach capacity, and climate resilience in nearby areas such as Somo (Cantabria) [83]. In this context, the observed trends in wave parameters and storm metrics may influence surf conditions, beach usability, and the temporal distribution of tourism demand, highlighting the broader socio-economic relevance of wave climate studies.

6. Conclusions

This study evaluates the effect of the record length on the stability of trend detection and extreme value estimates in offshore wave conditions in the Bay of Biscay.

Extreme value estimates are robust and more reliable for the longer M1 record, with small RL50 sensitivity to ± 0.5 m variations in u. In contrast, the shorter M2 record exhibits substantially greater dependence on threshold selection, reinforcing that storm characterization and design level inference are structurally more uncertain when derived from limited temporal coverage.

The results show no statistically significant trend is found in monthly H_S. Nevertheless, in the 32-year record, significant trends are identified in storm-related metrics, peak period, and wave steepness. In particular, storm frequency and storm power show a statistically significant increase. Alternatively, the shorter record yields to less consistent signals, illustrating how record length influences the trend detection, and how extreme wave climate change may become apparent through modifications in storminess and other wave variables rather than through monotonic changes in H_S.

From a spectral perspective, the absence of significant long-term change in monthly H_S suggests that total variance remains broadly stable, while the significant decrease in T_P together with the increase in S points to changes in wave spectral characteristics. Although the climate indices are derived from sea-level pressures rather than wind fields, their variability may reflect changes in storm tracks and prevailing wind regimes. In this context, the concurrent decrease in T_P and increase in steepness may be related to a relative strengthening of locally generated wind–sea conditions compared to long-period swell. However, this interpretation should be regarded as a working hypothesis for future work, since no spectral partitioning or wind–field analysis was performed in the present study.

Overall, the comparison between long and short records further confirms the strong dependence of extreme value and trend diagnostics on record duration. This has direct implications for coastal engineering applications, where design wave conditions and return levels are often derived from relatively short observational records, potentially leading to either over- or under-conservative estimates if uncertainty is not explicitly accounted for.

Correlation analyses indicate that regional wave variability is predominantly modulated by North Atlantic atmospheric modes, with the EA pattern emerging as the most consistent driver and NAO acting as a secondary modulator. ENSO does not appear as primary control in this region and manifests only as a weak, delayed signal detectable more clearly in the longer record. Notably, T_P responds more consistently to these atmospheric variabilities than H_S, supporting the interpretation that large-scale forcing alters wave spectral structure and storm characteristics without necessarily producing monotonic changes in H_S.

The observed increase in storminess metrics and the shift toward steeper offshore wave conditions suggest a propensity toward more impact-prone wave states in the nearshore. This implies that relying exclusively on H_S may underestimate structurally relevant changes in coastal hazards. Incorporating T_P and S into coastal-risk assessments and linking offshore trends with nearshore processes should be taken into consideration.

Taken together, the main findings are:

- Extreme value inference is highly sensitive to record length and threshold selection.
- Storminess metrics and spectral parameters provide more robust signals of climate variability than H_S alone.
- Regional wave variability is consistently associated with large-scale atmospheric forcing, underscoring the need for long-term observations in climate-scale assessments and coastal engineering design.

Supplementary Materials: The following supporting information can be downloaded at: https://www.mdpi.com/article/10.3390/jmse14070646/s1, Figure S1: Mean residual life plot used to support threshold selection for (a) M1 and (b) M2. The solid line shows the mean excess over threshold and the dashed lines indicate the 95% confidence interval; Table S1: Lag-1 autocorrelation coefficients for monthly wave parameters and climate indices at M1 and M2 buoys; Table S2: Pearson correlation coefficients between monthly aggregated wave parameters from the M1 and M2 buoys over the overlapping period 2007–2018. All correlations are statistically significant at the 95% confidence level.

Author Contributions: Conceptualization, M.V., C.M. and B.C.; methodology, M.V. and C.M.; software, M.V.; validation, M.V., C.M., F.C.-V., B.C., M.M. and A.S.-A.; formal analysis, M.V. and C.M.; investigation, M.V. and C.M.; resources, M.V., C.M. and F.C.-V.; data curation, M.V.; writing—original draft preparation, M.V. and C.M.; writing—review and editing, M.V., C.M., F.C.-V., B.C., M.M. and A.S.-A.; visualization, M.V. and C.M.; supervision, M.V., C.M., F.C.-V., B.C., M.M. and A.S.-A.; project administration, C.M.; funding acquisition, C.M. and A.S.-A. All authors have read and agreed to the published version of the manuscript.

Funding: This work has received funding from the European Union's Horizon 2020 research and innovation programme under grant agreement No. 101037097 (REST-COAST project).

Data Availability Statement: The Bilbao-Vizcaya buoy data (M1) are publicly available through the Puertos del Estado database (https://portus.puertos.es/#/, accessed on 24 January 2026), and the atmospheric indices (NAO, EA and ENSO) are openly accessible from the NOAA Climate Prediction Center and Physical Sciences Laboratory repositories (https://www.cpc.ncep.noaa.gov/data/teledoc/telecontents.shtml, accessed on 20 January 2026). The Augusto González de Linares buoy data (M2) were provided for research purposes under an institutional agreement and are not publicly available. Requests regarding these data should be directed to Manuel Viñes, manuel.vines@upc.edu.

Acknowledgments: The authors also wish to acknowledge the BARRACLIM project ("Barraques Climàtiques per adaptar la costa i les seves activitats a condicions futures"), funded by the Generalitat de Catalunya, Departament d'Acció Climàtica, Alimentació i Agenda Rural (Reference No. ACC_2023_EXP_SIA002_09_0001569). Second, the Departament de Recerca i Universitats de la Generalitat de Catalunya (Ref. Convocatoria d'ajuts a Grups de Recerca Catalunya (SGR-Cat 2021) 2021SGR00600), who supported the research group, and finally, Raquel Somavilla from the Spanish Institute of Oceanography for providing M2 data, and the technical assistance for the environmental monitoring of the sand extraction project in the northern sector of Zone II of the Port Authority of Bilbao, and of the central breakwater project for the extension of the Port of Bilbao in the Outer Abra (2022–2026).

Conflicts of Interest: The authors declare no conflicts of interest.

Abbreviations

The following abbreviations are used in this manuscript:

H_S	Significant Wave Height [m]
T_P	Wave Peak Period [s]
S	Wave Steepness
H	Wave Height [m]
L	Wavelength [m]
Tr	Return period [years]
u	Threshold value
POT	Peak Over Threshold method
MRL	Mean Residual Life plot
RL50	Return Level at 50 years
CI	Confidence Interval
CDF	Cumulative Distribution Function
GPD	Generalized Pareto Distribution
MLE	Maximum Likelihood Estimation
AC1	Lag 1 Autocorrelation Coefficient
MK	Mann–Kendall test
YW	Yue-Wang test
HR	Hamed-Rao test
AIC	Akaike Information Criterion
AICc	Corrected Akaike Information Criterion
QQ	Quantile-Quantile plot
NAO	North Atlantic Oscillation
EA	East Atlantic
ENSO	El Niño-Southern Oscillation
M1	Bilbao-Vizcaya buoy
M2	Augusto González de Linares buoy
PdE	Puertos del Estado
IEO	Instituto Español de Oceanografía
NOAA	National Oceanic and Atmospheric Administration

References

1. Mosso, C.; Mestres, M.; Sierra, J.P.; Sánchez-Arcilla, A.; Goodess, C. Waves and Surges in the Valencia Gulf. Variability Rather Than Climate Change. *J. Coast. Res.* **2009**, *1*, 243–247.
2. Mosso, C.; Viñes, M.; Astudillo, C.; Gracia, V.; González, D.; Calderón-Vega, F.; Sierra, J.P.; Sánchez-Arcilla, A. Assessing Coastal Flood Risk Under Climate Change with Public Data and Simple Tools: The Geomorphological Coastal Flood Index Applied to the Western Mediterranean. *Coasts* **2025**, *5*, 42. [CrossRef]
3. Calvillo, B.; Pavo-Fernández, E.; Grifoll, M.; Gracia, V. Automated Detection of Submerged Sandbar Crest Using Sentinel-2 Imagery. *Remote Sens.* **2025**, *18*, 132. [CrossRef]
4. Castelle, B.; Dodet, G.; Masselink, G.; Scott, T. Increased Winter-Mean Wave Height, Variability, and Periodicity in the Northeast Atlantic Over 1949–2017. *Geophys. Res. Lett.* **2018**, *45*, 3586–3596. [CrossRef]
5. Masselink, G.; Castelle, B.; Scott, T.; Konstantinou, A. Role of Atmospheric Indices in Describing Shoreline Variability Along the Atlantic Coast of Europe. *Geophys. Res. Lett.* **2023**, *50*, e2023GL106019. [CrossRef]
6. Grifoll, M.; Fontán, A.; Ferrer, L.; Mader, J.; González, M.; Espino, M. 3D Hydrodynamic Characterisation of a Meso-Tidal Harbour: The Case of Bilbao (Northern Spain). *Coast. Eng.* **2009**, *56*, 907–918. [CrossRef]
7. Omonigbehin, O.; Eresanya, E.O.; Tao, A.; Setordjie, V.E.; Daramola, S.; Adebiyi, A. Long-Term Evolution of Significant Wave Height in the Eastern Tropical Atlantic between 1940 and 2022 Using the ERA5 Dataset. *J. Mar. Sci. Eng.* **2024**, *12*, 714. [CrossRef]
8. Xu, W.; Chen, S.; Ji, H.; Hu, T.; Zhong, X.; Li, P. Dynamics of Sandy Shorelines and Their Response to Wave Climate Change in the East of Hainan Island, China. *J. Mar. Sci. Eng.* **2024**, *12*, 1921. [CrossRef]
9. Viñes, M.; Sánchez-Arcilla, A.; Epelde, I.; Mösso, C.; Franco, J.; Sospedra, J.; Abalia, A.; Líria, P.; Grifoll, M.; Ojanguren, A.; et al. Morphodynamic Predictions Based on Machine Learning. Performance and Limits for Pocket Beaches near the Bilbao Port. *Front. Environ. Sci.* **2025**, *13*, 473. [CrossRef]
10. Prestes, Y.O.; da Silva, A.C.; Marquez, A.L.; Gomes Junior, G.D.; Hernandez, F. Climate Variability and Atlantic Surface Gravity Wave Variability Based on Reanalysis Data. *J. Mar. Sci. Eng.* **2025**, *13*, 1536. [CrossRef]
11. Rasilla, D.; García-Codron, J.C.; Garmendia, C.; Herrera, S.; Rivas, V. Extreme Wave Storms and Atmospheric Variability at the Spanish Coast of the Bay of Biscay. *Atmosphere* **2018**, *9*, 316. [CrossRef]
12. Kuriyama, Y.; Banno, M.; Suzuki, T. Linkages among Interannual Variations of Shoreline, Wave and Climate at Hasaki, Japan. *Geophys. Res. Lett.* **2012**, *39*, 6604. [CrossRef]
13. Castelle, B.; Kras, E.; Masselink, G.; Scott, T.; Konstantinou, A.; Luijendijk, A. Satellite-Derived Sandy Shoreline Trends and Interannual Variability along the Atlantic Coast of Europe. *Sci. Rep.* **2024**, *14*, 13002. [CrossRef] [PubMed]
14. Dupuis, H.; Michel, D.; Sottolichio, A. Wave Climate Evolution in the Bay of Biscay over Two Decades. *J. Mar. Syst.* **2006**, *63*, 105–114. [CrossRef]
15. Charles, E.; Idier, D.; Thiébot, J.; Le Cozannet, G.; Pedreros, R.; Ardhuin, F.; Planton, S. Present Wave Climate in the Bay of Biscay: Spatiotemporal Variability and Trends from 1958 to 2001. *J. Clim.* **2012**, *25*, 2020–2039. [CrossRef]
16. Camus, P.; Mendez, F.J.; Medina, R. A Hybrid Efficient Method to Downscale Wave Climate to Coastal Areas. *Coast. Eng.* **2011**, *58*, 851–862. [CrossRef]
17. Ibeas, M.; Martínez-Marrero, A. Long-Term Trends, Interannual Variability and Seasonal Patterns of Mean Sea Level in the Canary Islands. *J. Mar. Sci. Eng.* **2025**, *13*, 2193. [CrossRef]
18. Bromirski, P.D.; Cayan, D.R. Wave Power Variability and Trends Across The North Atlantic Influenced by Decadal Climate Patterns. *J. Geophys. Res. Ocean.* **2015**, *120*, 3419–3443. [CrossRef]
19. Thornton, H.E.; Smith, D.M.; Scaife, A.A.; Dunstone, N.J. Seasonal Predictability of the East Atlantic Pattern in Late Autumn and Early Winter. *Geophys. Res. Lett.* **2023**, *50*, e2022GL100712. [CrossRef]
20. Casselman, J.W.; Jiménez-Esteve, B.; Domeisen, D.I.V. Modulation of the El Niño Teleconnection to the North Atlantic by the Tropical North Atlantic during Boreal Spring and Summer. *Weather Clim. Dyn.* **2022**, *3*, 1077–1096. [CrossRef]
21. Rodríguez-Fonseca, B.; Suárez-Moreno, R.; Ayarzagüena, B.; López-Parages, J.; Gómara, I.; Villamayor, J.; Mohino, E.; Losada, T.; Castaño-Tierno, A. A Review of ENSO Influence on the North Atlantic. A Non-Stationary Signal. *Atmosphere* **2016**, *7*, 87. [CrossRef]
22. González-Marco, D.; Sánchez-Arcilla, A.; Panagiotis, P. Analysis of extremes for hazard assessment. In Proceedings of the 32nd IAHR World Congress 2007, Venice, Italy, 1–6 July 2007.
23. Katalinić, M.; Parunov, J. Uncertainties of Estimating Extreme Significant Wave Height for Engineering Applications Depending on the Approach and Fitting Technique—Adriatic Sea Case Study. *J. Mar. Sci. Eng.* **2020**, *8*, 259. [CrossRef]
24. Calderón-Vega, F.; García-Soto, A.-D.; Mösso, C. Correlation of Concurrent Extreme Metocean Hazards Considering Seasonality. *Appl. Sci.* **2020**, *10*, 4794. [CrossRef]
25. Holthuijsen, L.H. *Waves in Oceanic and Coastal Waters*; Cambridge University Press: Cambridge, UK, 2007; ISBN 9780521860284.
26. Young, I.R. *Wind Generated Ocean Waves*; Elsevier: Amsterdam, The Netherlands, 1999; p. 307.

27. Gorostiaga, J.; Díez, I. Changes in the Sublittoral Benthic Marine Macroalgae in the Polluted Area of Abra de Bilbao and Proximal Coast (Northern Spain). *Mar. Ecol. Prog. Ser.* **1996**, *130*, 157–167. [CrossRef]
28. Mösso, C.; Mestres, M.; Sierra, J.P. Evaluation of Wave Energy and Tidal Stream Resources in Bilbao (N Spain). In Proceedings of the 11th European Wave and Tidal Energy Conference (EWTEC), Nantes, France, 6–11 September 2015.
29. de Santiago, I.; Camus, P.; González, M.; Liria, P.; Epelde, I.; Chust, G.; del Campo, A.; Uriarte, A. Impact of Climate Change on Beach Erosion in the Basque Coast (NE Spain). *Coast. Eng.* **2021**, *167*, 103916. [CrossRef]
30. Basterretxea-Iribar, I.; Sotés, I.; Maruri, M.D.L.M. Managing Bathers' Capacity at Overcrowded Beaches: A Case on the Spanish North Atlantic Coast. *Tour. Manag.* **2019**, *71*, 453–465. [CrossRef]
31. Sánchez-Arcilla, A.; Lin-Ye, J.; García-León, M.; Gràcia, V.; Pallarès, E. The Land-Sea Coastal Border: A Quantitative Definition by Considering the Wind and Wave Conditions in a Wave-Dominated, Micro-Tidal Environment. *Ocean Sci.* **2019**, *15*, 113–126. [CrossRef]
32. Meng, Z.; Chen, Y.; Liu, Y.; Ding, Y. Mooring Stability Study for Novel Wave Energy Converter Based on Regular Wave. *J. Mar. Sci. Eng.* **2021**, *9*, 1095. [CrossRef]
33. Liu, G.; Ouyang, Q.; He, Z.; Zhang, N. The Application of a Joint Distribution of Significant Wave Heights and Peak Wave Periods in the Northwestern South China Sea. *J. Mar. Sci. Eng.* **2025**, *13*, 570. [CrossRef]
34. You, Z.-J. A Close Approximation of Wave Dispersion Relation for Direct Calculation of Wavelength in Any Coastal Water Depth. *Appl. Ocean Res.* **2008**, *30*, 113–119. [CrossRef]
35. Iglesias, I.; Lorenzo, M.N.; Taboada, J.J. Seasonal Predictability of the East Atlantic Pattern from Sea Surface Temperatures. *PLoS ONE* **2014**, *9*, e86439. [CrossRef]
36. Portis, D.H.; Walsh, J.E.; Hamly, M.E.l.; Lamb, P.J. Seasonality of the North Atlantic Oscillation. *J. Clim.* **2001**, *14*, 2069–2078. [CrossRef]
37. Hilton, D.; Davidson, M.; Scott, T. Seasonal Predictions of Shoreline Change, Informed by Climate Indices. *J. Mar. Sci. Eng.* **2020**, *8*, 616. [CrossRef]
38. NOAA Center for Weather and Climate Prediction Climate Prediction Center: North Atlantic Oscillation (NAO) Index. Available online: https://www.ncei.noaa.gov/access/monitoring/nao/ (accessed on 20 January 2026).
39. NOAA Center for Weather and Climate Prediction Climate Prediction Center—East Atlantic Pattern (EA) Index. Available online: https://www.cpc.ncep.noaa.gov/data/teledoc/ea.shtml (accessed on 20 January 2026).
40. Aravena, G.; Villate, F.; Iriarte, A.; Uriarte, I.; Ibáñez, B. Influence of the North Atlantic Oscillation (NAO) on Climatic Factors and Estuarine Water Temperature on the Basque Coast (Bay of Biscay): Comparative Analysis of Three Seasonal NAO Indices. *Cont. Shelf Res.* **2009**, *29*, 750–758. [CrossRef]
41. Lin-Ye, J.; Garcia-Leon, M.; Gracia, V.; Sanchez-Arcilla, A. A Multivariate Statistical Model of Extreme Events: An Application to the Catalan Coast. *Coast. Eng.* **2016**, *117*, 138–156. [CrossRef]
42. Harley, M. Coastal Storm Definition. In *Coastal Storms*; Wiley: Hoboken, NJ, USA, 2017; pp. 1–21.
43. Faranda, D.; Lucarini, V.; Turchetti, G.; Vaienti, S. Numerical Convergence of the Block-Maxima Approach to the Generalized Extreme Value Distribution. *J. Stat. Phys.* **2011**, *145*, 1156–1180. [CrossRef]
44. Coles, S. *An Introduction to Statistical Modeling of Extreme Values*; Springer: London, UK, 2001. [CrossRef]
45. Larsén, X.G.; Kalogeri, C.; Galanis, G.; Kallos, G. A Statistical Methodology for the Estimation of Extreme Wave Conditions for Offshore Renewable Applications. *Renew. Energy* **2015**, *80*, 205–218. [CrossRef]
46. Puertos del Estado. *Análisis Clima Extremal Boya Bilbao-Vizcaya*; Puertos del Estado: Madrid, Spain, 2020.
47. Embrechts, P.; Klüppelberg, C.; Mikosch, T. *Modelling Extremal Events*; Springer: Berlin/Heidelberg, Germany, 1997; ISBN 978-3-642-08242-9.
48. Takbash, A.; Young, I. Long-Term and Seasonal Trends in Global Wave Height Extremes Derived from ERA-5 Reanalysis Data. *J. Mar. Sci. Eng.* **2020**, *8*, 1015. [CrossRef]
49. Liu, C.; Jia, Y.; Onat, Y.; Cifuentes-Lorenzen, A.; Ilia, A.; McCardell, G.; Fake, T.; O'Donnell, J. Estimating the Annual Exceedance Probability of Water Levels and Wave Heights from High Resolution Coupled Wave-Circulation Models in Long Island Sound. *J. Mar. Sci. Eng.* **2020**, *8*, 475. [CrossRef]
50. Ballester, J.; van Daalen, K.R.; Chen, Z.Y.; Achebak, H.; Antó, J.M.; Basagaña, X.; Robine, J.M.; Herrmann, F.R.; Tonne, C.; Semenza, J.C.; et al. The Effect of Temporal Data Aggregation to Assess the Impact of Changing Temperatures in Europe: An Epidemiological Modelling Study. *Lancet Reg. Health—Eur.* **2024**, *36*, 100779. [CrossRef]
51. Hong, B.; Zhang, J. Long-Term Trends of Sea Surface Wind in the Northern South China Sea under the Background of Climate Change. *J. Mar. Sci. Eng.* **2021**, *9*, 752. [CrossRef]
52. Yang, Z.; Niu, X. Trends of Extreme Waves around Hainan Island during Typhoon Processes. *Ocean Eng.* **2024**, *308*, 118247. [CrossRef]
53. Nguyen, H.M.; Ouillon, S.; Vu, V.D. Sea Level Variation and Trend Analysis by Comparing Mann–Kendall Test and Innovative Trend Analysis in Front of the Red River Delta, Vietnam (1961–2020). *Water* **2022**, *14*, 1709. [CrossRef]

54. Guevara Díaz, J.M. Uso Correcto de La Correlación Cruzada En Climatología: El Caso de La Presión Atmosférica Entre Taití y Darwin. *Terra Nueva Etapa* **2014**, *30*, 79–102.
55. Hunt, N. Chapter 8: Autocorrelation Function, Mutual Information, and Correlation Dimension. *Dep. Biomech.* **2016**, 301–341.
56. Yue, S.; Wang, C. The Mann-Kendall Test Modified by Effective Sample Size to Detect Trend in Serially Correlated Hydrological Series. *Water Resour. Manag.* **2004**, *18*, 201–218. [CrossRef]
57. Hamed, K.H.; Ramachandra Rao, A. A Modified Mann-Kendall Trend Test for Autocorrelated Data. *J. Hydrol.* **1998**, *204*, 182–196. [CrossRef]
58. Nauleau, P.; Apostolakis, I.; McGarry, M.; Konofagou, E. Cross-Correlation Analysis of Pulse Wave Propagation in Arteries: In Vitro Validation and in Vivo Feasibility. *Phys. Med. Biol.* **2018**, *63*, 115006. [CrossRef]
59. Wisha, U.J.; Wijaya, Y.J.; Hisaki, Y. Sea Level Variability in the Equatorial Malacca Strait: The Influence of Climatic–Oceanographic Factors and Its Implications for Tidal Properties in the Estuarine Zone. *Climate* **2023**, *11*, 70. [CrossRef]
60. Dodet, G.; Bertin, X.; Taborda, R. Wave Climate Variability in the North-East Atlantic Ocean over the Last Six Decades. *Ocean Model.* **2010**, *31*, 120–131. [CrossRef]
61. Bertin, X.; Prouteau, E.; Letetrel, C. A Significant Increase in Wave Height in the North Atlantic Ocean over the 20th Century. *Glob. Planet. Change* **2013**, *106*, 77–83. [CrossRef]
62. Le Cozannet, G.; Lecacheux, S.; Delvallee, E.; Desramaut, N.; Oliveros, C.; Pedreros, R. Teleconnection Pattern Influence on Sea-Wave Climate in the Bay of Biscay. *J. Clim.* **2011**, *24*, 641–652. [CrossRef]
63. Forkel, M.; Carvalhais, N.; Verbesselt, J.; Mahecha, M.; Neigh, C.; Reichstein, M. Trend Change Detection in NDVI Time Series: Effects of Inter-Annual Variability and Methodology. *Remote Sens.* **2013**, *5*, 2113–2144. [CrossRef]
64. Hardison, S.; Perretti, C.T.; DePiper, G.S.; Beet, A. A Simulation Study of Trend Detection Methods for Integrated Ecosystem Assessment. *ICES J. Mar. Sci.* **2019**, *76*, 2060–2069. [CrossRef]
65. Jordà, G. Detection Time for Global and Regional Sea Level Trends and Accelerations. *J. Geophys. Res. Ocean.* **2014**, *119*, 7164–7174. [CrossRef]
66. Casas-Prat, M.; Wang, X.L.; Mori, N.; Feng, Y.; Chan, R.; Shimura, T. Effects of Internal Climate Variability on Historical Ocean Wave Height Trend Assessment. *Front. Mar. Sci.* **2022**, *9*, 847017. [CrossRef]
67. García-Soto, A.-D.; Calderón-Vega, F.; Mösso, C.; Valdés-Vázquez, J.-G.; Hernández-Martínez, A. Revisiting Two Simulation-Based Reliability Approaches for Coastal and Structural Engineering Applications. *Appl. Sci.* **2020**, *10*, 8176. [CrossRef]
68. Vanem, E. Uncertainties in Extreme Value Modelling of Wave Data in a Climate Change Perspective. *J. Ocean Eng. Mar. Energy* **2015**, *1*, 339–359. [CrossRef]
69. Bitner-Gregersen, E.M.; Waseda, T.; Parunov, J.; Yim, S.; Hirdaris, S.; Ma, N.; Guedes Soares, C. Uncertainties in Long-Term Wave Modelling. *Mar. Struct.* **2022**, *84*, 103217. [CrossRef]
70. Jamous, M.; Marsooli, R. A Multidecadal Assessment of Mean and Extreme Wave Climate Observed at Buoys off the U.S. East, Gulf, and West Coasts. *J. Mar. Sci. Eng.* **2023**, *11*, 916. [CrossRef]
71. Wolf, J.; Woolf, D.K. Waves and Climate Change in the North-east Atlantic. *Geophys. Res. Lett.* **2006**, *33*, L06604. [CrossRef]
72. Stansberg, C.T. Wave Front Steepness and Influence on Horizontal Deck Impact Loads. *J. Mar. Sci. Eng.* **2020**, *8*, 314. [CrossRef]
73. Feliks, Y.; Ghil, M.; Robertson, A.W. The Atmospheric Circulation over the North Atlantic as Induced by the SST Field. *J. Clim.* **2011**, *24*, 522–542. [CrossRef]
74. Martínez-Asensio, A.; Tsimplis, M.N.; Marcos, M.; Feng, X.; Gomis, D.; Jordà, G.; Josey, S.A. Response of the North Atlantic Wave Climate to Atmospheric Modes of Variability. *Int. J. Climatol.* **2016**, *36*, 1210–1225. [CrossRef]
75. Cañellas, B.; Orfila, A.; Méndez, F.; Álvarez, A.; Tintoré, J. Influence of the NAO on the Northwestern Mediterranean Wave Climate. *Sci. Mar.* **2010**, *74*, 55–64. [CrossRef]
76. Hannachi, A.; Jolliffe, I.T.; Stephenson, D.B. Empirical Orthogonal Functions and Related Techniques in Atmospheric Science: A Review. *Int. J. Climatol.* **2007**, *27*, 1119–1152. [CrossRef]
77. Mezzina, B.; García-Serrano, J.; Ambrizzi, T.; Matei, D.; Manzini, E.; Bladé, I. Tropospheric Pathways of the Late-Winter ENSO Teleconnection to Europe. *Clim. Dyn.* **2023**, *60*, 3307–3317. [CrossRef]
78. Klein, S.A.; Soden, B.J.; Lau, N.-C. Remote Sea Surface Temperature Variations during ENSO: Evidence for a Tropical Atmospheric Bridge. *J. Clim.* **1999**, *12*, 917–932. [CrossRef]
79. García-Serrano, J.; Cassou, C.; Douville, H.; Giannini, A.; Doblas-Reyes, F.J. Revisiting the ENSO Teleconnection to the Tropical North Atlantic. *J. Clim.* **2017**, *30*, 6945–6957. [CrossRef]
80. Mezzina, B.; García-Serrano, J.; Bladé, I.; Kucharski, F. Dynamics of the ENSO Teleconnection and NAO Variability in the North Atlantic–European Late Winter. *J. Clim.* **2020**, *33*, 907–923. [CrossRef]
81. Jiménez-Esteve, B.; Domeisen, D.I.V. Nonlinearity in the Tropospheric Pathway of ENSO to the North Atlantic. *Weather Clim. Dyn.* **2020**, *1*, 225–245. [CrossRef]

82. Sánchez-Artús, X.; Gracia, V.; Espino, M.; Sierra, J.P.; Pinyol, J.; Sánchez-Arcilla, A. Present and Future Flooding and Erosion along the NW Spanish Mediterranean Coast. *Front. Mar. Sci.* **2023**, *10*, 1125138. [CrossRef]
83. Boqué Ciurana, A.; Ménendez, M.; Suárez Bilbao, M.; Aguilar, E. Exploring the Climatic Potential of Somo's Surf Spot for Tourist Destination Management. *Sustainability* **2022**, *14*, 8496. [CrossRef]

Disclaimer/Publisher's Note: The statements, opinions and data contained in all publications are solely those of the individual author(s) and contributor(s) and not of MDPI and/or the editor(s). MDPI and/or the editor(s) disclaim responsibility for any injury to people or property resulting from any ideas, methods, instructions or products referred to in the content.